Cirrus Cloud Properties from a Cloud-Resolving Model Simulation Compared to Cloud Radar Observations

YALI LUO, STEVEN K. KRUEGER, AND GERALD G. MACE

Department of Meteorology, University of Utah, Salt Lake City, Utah

KUAN-MAN XU

NASA Langley Research Center, Hampton, Virginia

(Manuscript received 26 September 2001, in final form 13 June 2002)

ABSTRACT

Cloud radar data collected at the Atmospheric Radiation Measurement (ARM) Program's Southern Great Plains site were used to evaluate the properties of cirrus clouds that occurred in a cloud-resolving model (CRM) simulation of the 29-day summer 1997 intensive observation period (IOP). The simulation was ''forced'' by the large-scale advective temperature and water vapor tendencies, horizontal wind velocity, and turbulent surface fluxes observed at the Southern Great Plains site. The large-scale advective condensate tendency was not observed. The correlation of CRM cirrus amount with Geostationary Operational Environmental Satellite (GOES) high cloud amount was 0.70 for the subperiods during which cirrus formation and decay occurred primarily locally, but only 0.30 for the entire IOP. This suggests that neglecting condensate advection has a detrimental impact on the ability of a model (CRM or single-column model) to properly simulate cirrus cloud occurrence.

The occurrence, vertical location, and thickness of cirrus cloud layers, as well as the bulk microphysical properties of thin cirrus cloud layers, were determined from the cloud radar measurements for June, July, and August 1997. The composite characteristics of cirrus clouds derived from this dataset are well suited for evaluating CRMs because of the close correspondence between the timescales and space scales resolved by the cloud radar measurements and by CRMs. The CRM results were sampled at eight grid columns spaced 64 km apart using the same definitions of cirrus and thin cirrus as the cloud radar dataset. The composite characteristics of cirrus clouds obtained from the CRM were then compared to those obtained from the cloud radar.

Compared with the cloud radar observations, the CRM cirrus clouds occur at lower heights and with larger physical thicknesses. The ice water paths in the CRM's thin cirrus clouds are similar to those observed. However, the corresponding cloud-layer-mean ice water contents are significantly less than observed due to the CRM's larger cloud-layer thicknesses. The strong dependence of cirrus microphysical properties on layer-mean temperature and layer thickness as revealed by the observations is reproduced by the CRM. In addition, both the CRM and the observations show that the thin cirrus ice water path during large-scale ascent is only slightly greater than during no ascent or descent.

1. Introduction

Cirrus clouds, because of their frequent occurrence and large coverage globally, strongly influence weather and climate processes through their effects on the radiation budget of the earth and the atmosphere (Liou 1986). Located high in the troposphere and composed of nonspherical ice crystals of various shapes, their representation in numerical weather prediction models and general circulation models (GCMs) has been identified as one of the greatest uncertainties in weather and climate research.

A cloud-resolving model (CRM) is a numerical model that resolves cloud-scale (and mesoscale) circulations in either two or three spatial dimensions. CRMs have been widely used in cloud system research to investigate the formation, maintenance, structure, and dissipation of cloud systems (e.g., Xu et al. 1992; Krueger et al. 1995a,b), to test and develop cloud parameterizations (e.g., Xu and Krueger 1991; Xu and Arakawa 1992; Xu and Randall 1996; Köhler 1999), and to evaluate the sensitivity of model results to parameter changes. In addition to the observations and single-column models (SCMs), CRMs are the primary tools of the Global Energy and Water Cycle Experiment (GEWEX) Cloud Systems Study (GCSS; Browning 1993) and the Atmospheric Radiation Measurement (ARM; Stokes and Schwartz 1994) Program. CRMs may be increasingly used in GCMs to replace the cumulus and stratiform cloud parameterizations (e.g., Khairoutdinov and Rand-

Corresponding author address: Yali Luo, Department of Meteorology, University of Utah, 135 South 1460 East, Room 819, Salt Lake City, UT 84112-0110.
E-mail: yali@met.utah.edu.

all 2001). Thus, evaluating the representation of cirrus clouds in a CRM will soon be considered part of evaluating GCMs.

A few studies have been made to evaluate the representation of tropical cirrus clouds in CRMs (Brown and Heymsfield 2001; Krueger et al. 1995c; Fu et al. 1995), mainly due to the limited number of suitable observational datasets. Brown and Heymsfield (2001) statistically evaluated the microphysical properties of tropical convective anvil cirrus simulated by a 2D CRM by comparing with aircraft-measured data. The model was found to represent the distribution of total ice water content (IWC) quite well and, for temperatures warmer than −40°C, to correctly predict the dominant contribution of large particles to the IWC. At colder temperatures, the model overestimated the fraction of IWC in large particles and the predicted maximum crystal length exceeded the observed values in this temperature range. Sensitivity tests suggested that the excessive rates of autoconversion and aggregation of cloud ice partly caused the discrepancies found. Krueger et al. (1995c) increased the amount of cloud ice and the extent of tropical anvil clouds simulated by a CRM by improving its microphysics. Fu et al. (1995) showed that these modifications improved the microphysics parameterization by comparing the predicted steady-state IWC as a function of vertical velocity and temperature to the measurements used by Heymsfield and Donner (1990) to evaluate their IWC parameterization.

Evaluation of midlatitude cirrus clouds in CRMs is very limited due to, again, lack of observations. Recently, the continuous cloud radar measurements at the ARM Southern Great Plains (SGP) site have produced extensive datasets. Based on these data, Mace et al. (2001, MCA hereafter) examined the statistical properties of cirrus clouds. These are very new statistics about midlatitude cirrus clouds and make CRM evaluation possible. During the ARM summer 1997 single-column model intensive observation period (IOP), many high clouds were observed over the SGP site. This period offers a good opportunity to evaluate the cirrus physics in CRMs.

It is increasingly recognized in the numerical weather prediction and the global climate modeling communities that compositing techniques allow evaluation of cloud physical processes while removing the impact of possible errors in the large-scale circulation (e.g., Bony et al. 1997; Lau and Crane 1997; Klein and Jakob 1999; Tselioudis et al. 2000; Norris and Weaver 2001).

The compositing approach has most commonly been based on satellite cloud observations over a large area. Ground-based cloud radar observations are similar to geostationary satellite observations for a single location, with some important differences. Whereas a satellite can retrieve quantities such as cloud-top pressure and optical depth at cloud-scale resolution (0.5 h, 4 km), the ARM SGP cloud radar can determine the vertical location and extent of cloud layers with an accuracy of 90 m every 36 s within a vertical beam that is 33 m in diameter at 10 km above the surface. In addition, methods have been developed to use cloud radar measurements to retrieve bulk microphysical properties of various cloud types, including thin cirrus (e.g., MCA). A time series of such measurements is able to characterize the subcloud-scale variability that is produced by interacting cloud processes (dynamics, microphysics, and radiative transfer). Such cloud characteristics, when appropriately composited, can aid the evaluation and improvement of cirrus parameterizations in large-scale models, as noted by MCA. However, they are equally valuable, and perhaps easier to utilize, for evaluating CRMs, because of the close correspondence between the time and space scales resolved by the cloud radar measurements and by a CRM.

To fully utilize cloud radar–derived or satellite-derived composite cloud characteristics when evaluating a GCM or an SCM, one must first create a synthetic cloud field from the model's large-scale cloud variables (cloud water/ice mixing ratio and cloud fraction) based on the model's assumptions about subgrid-scale cloud variability and overlap (e.g., Klein and Jakob 1999). We have used this approach to evaluate the cirrus properties simulated by an SCM (Luo et al. 2002).

In this paper, we compare the composite characteristics of cirrus clouds that occurred in a CRM simulation, which was driven by the ARM analysis for the summer 1997 SCM IOP, with radar observations and results from a retrieval of cirrus properties using combined radar and interferometer data (MCA). The performance of CRMs, including the CRM used, driven by the same dataset was analyzed by Xu and Randall (2000) and Xu et al. (2002). Many aspects of the simulation, such as surface precipitation, precipitable water, and profiles of temperature, specific humidity, cloud mass flux, condensate mixing ratio, and hydrometer fraction were studied. However, they did not look at the simulated cirrus physics, particularly in a statistical way. To avoid duplication, we will focus on the simulated cirrus cloud information in our analysis. Section 2 is a brief description of the CRM that we used and the simulation we analyzed. In section 3, we first describe the cirrus retrieval used for comparison. This is followed by an explanation of the method used to sample cirrus clouds in the CRM simulations. In section 4, we present a statistical comparison of the simulated and retrieved cirrus properties. Various properties are compared including cirrus cloud occurrence frequency (COF), cirrus cloud base and top height, cloud thickness, layer mean temperature, ice water content (IWC), ice water path (IWP), and equivalent spherical effective radius of ice crystals (r_e), which is defined as the ratio of the third and second moments of the size distribution. The dependence of cirrus microphysical properties on temperature, cloud thickness, and large-scale vertical velocity is also examined. Section 5 contains our conclusions.

2. CRM simulations

a. UCLA–CSU cloud-resolving model

The cloud resolving model used in this study is the 2D University of California at Los Angeles–Colorado State University (UCLA–CSU) CRM. The details of the CRM have been described by Krueger (1988), Xu and Krueger (1991), and Xu and Randall (1995). The dynamics of the CRM are based on the anelastic system. The physical parameterizations in the model consist of a third-moment turbulence closure, a bulk three-phase microphysics, and an interactive solar and IR radiative transfer scheme. Turbulent surface fluxes are diagnosed using flux–profile relationships based on Monin–Obukhov surface-layer similarity theory (Businger et al. 1971). The radiation parameterization is based on the Harshvardhan et al. broadband radiative transfer model (Harshvardhan et al. 1987; Xu and Randall 1995) with cloud optical properties as formulated by Stephens et al. (1990).

The description of the bulk microphysics of the CRM can be found in Fu et al. (1995), Krueger et al. (1995c), Lord et al. (1984), Lin et al. (1983), and Hsie et al. (1980). The bulk microphysics includes five species: cloud water, cloud ice, snow, graupel, and rain. In the CRM, cirrus clouds contain small ice crystals (''cloud ice'') and large ice crystals (''snow''). The cloud ice in the model increases due to nucleation and depositional growth and decreases due to sublimation, conversion to snow, and accretion by snow and graupel. Within the model, the processes that generate snow are the collision and aggregation of the smaller cloud ice particles, contact freezing of small raindrops, and depositional growth and riming of small ice crystals. Once generated, the snow continues to grow by accretion and deposition. Sublimation and melting reduce the snow content. The ice microphysics scheme produces IWC values as a function of temperature and vertical velocity that are comparable to measurements presented by Heymsfield and Donner (1990; Fu et al. 1995).

According to numerical cirrus model results (Starr and Cox 1985), the vertical transport of ice due to sedimentation is very significant in cirrus. In the CRM, cloud water and cloud ice have zero fall speed, and snow, rain, and graupel have mass-weighted mean terminal velocities that depend on the mixing ratio and size distribution assumed. For snow, an exponential size distribution is hypothesized:

$$n_S(D) = n_{0S} \exp(-\lambda_S D_S), \tag{1}$$

where n_{0S} is the intercept parameter of the snow size distribution, D_S is diameter of the snow particles, and λ_S is the slope parameter of the snow size distribution. According to the measurements of Gunn and Marshall (1958), n_{0S} is given as 3×10^{-2} cm^{-4}. By multiplying (1) by particle mass and integrating over all diameters and equating the resulting quantity to the snow content, λ_S is determined. In the CRM, the terminal velocity of a snow particle of diameter D_S is

$$U_{DS} = cD_S^d \left(\frac{\rho_0}{\rho}\right)^{1/2}. \tag{2}$$

Fu et al. (1995) based this on the relation suggested by Locatelli and Hobbs (1974). Specifically, U_{DS} is appropriate for graupel-like snow of hexagonal type, with the constants c and d being 152.93 cm^{1-d} s^{-1} and 0.25, respectively. The square root factor involving air density ρ allows for increasing fall speeds with increasing altitude. The mass-weighted terminal velocity is defined as

$$U_S = \int U_{DS} q(D_S)\, dD_S / q_S, \tag{3}$$

where $q(D_S)dD_S$ is the mixing ratio of snow particles with diameters D_S, and q_S is the total mixing ratio of snow. Combining (1), (2), and (3), we obtain the mass-weighted mean terminal velocity of snow:

$$U_S = \frac{c\Gamma(4 + d)}{6\lambda_S^d} \left(\frac{\rho_0}{\rho}\right)^{1/2}. \tag{4}$$

In (4), Γ is the gamma function. We will discuss the effects of using this method of determining fall speed of snow on cirrus properties in the CRM in later sections.

b. Simulation description

We analyzed a 29-day simulation based on the large-scale dataset of the ARM summer 1997 single-column model intensive observation period at the SGP Cloud and Radiation Testbed (CART) site produced by the variational analysis method (Xu and Randall 2000). The domain size is 512 km by 18 km, with a horizontal grid size of 2 km and a variable vertical grid size that is about 800 m at cirrus levels. ARM analyses used by the simulation consist of initial atmospheric state, time-varying large-scale advective tendencies of potential temperature and water vapor, time-varying large-scale horizontal winds, time-varying surface turbulent fluxes, and time-varying surface pressure.

Balloon-borne soundings of winds, temperature, and dewpoint temperature were obtained every 3 h from the SGP CART central facility located near Lamont, Oklahoma (36.61°N, 97.49°W) and from four boundary facilities, which form a rectangle of approximately 300 km $\times$ 370 km. The sounding data, combined with the surface and the top-of-atmosphere flux observations, are analyzed over such a horizontal domain by Zhang and colleagues, using a constrained variational objective analysis method (Zhang and Lin 1997; Zhang et al. 2001). The variational analysis method forces the atmospheric state variables to satisfy conservations of mass, moisture, energy, and momentum by making small adjustments to the original soundings of winds,

temperature, and water vapor mixing ratio. The large-scale advective tendencies used to drive the CRM were obtained by averaging the constraining surface and the top-of-atmosphere flux observations over 9 h. This may produce some errors in the forcing. The averaged flux observations and the large-scale forcing obtained by using them are called version 1 here, and those that were not averaged are called version 2. We used both for our analysis of results in this study, but the simulation was based upon the version 1 dataset.

Observed surface turbulent fluxes from the ARM energy balance/Bowen ratio measurements were used in the CRM. The CRM surface fluxes are first calculated from surface turbulent flux formulations using the prescribed ground temperature and soil wetness. Then the difference between the observed flux and the CRM domain-averaged flux is added to the calculated flux, at each grid point, to get a new surface flux that is used in other parts of the model. By doing this, only the domain-averaged fluxes are constrained to the observed values and horizontal variations of the surface fluxes are allowed.

Also, the observed horizontal wind components are nudged with a nudging time of 1 h so that the domain-averaged horizontal wind components are approximately equal to the observed. The horizontal inhomogeneity of u and v components inside the CRM domain is preserved by the nudging procedure. Unfortunately, the large-scale horizontal advection of condensate is not included due to lack of measurements. In the upper troposphere, values of the divergence of hydrometers due to horizontal advection can be a similar order of magnitude as the divergence of water vapor, that is, 0.1 g kg^{-1} h^{-1} (Petch and Dudhia 1998). Periodic lateral boundary conditions are used. This is consistent with imposing horizontally uniform large-scale forcing. In the CRM, convection is initiated by introducing small random perturbations in the temperature field in the subcloud layer for the first hour or so. The interactions between clouds and radiation are included in the simulation.

During this IOP, clouds over SGP CART site were mainly high clouds as revealed by the time series of Geostationary Operational Environmental Satellite (GOES) total cloud amount and high-cloud amount (Fig. 1). By watching the animation of clouds observed by GOES,[1] we chose the subperiods A, B, and C during which cloud systems were mostly formed locally, and precipitation occurred most of the time. When we compare the CRM-simulated cirrus occurrence with GOES and radar-observed cirrus occurrence in section 4, we will look at both the entire IOP and the subset consisting of these three subperiods.

It was found that the evolution of convective activity, temperature, and specific humidity are reasonably simulated (Xu et al. 2002; Xu and Randall 2000). As a supplement, we provide a comparison of simulated relative humidity with the observed values (Fig. 2). At upper troposphere, the root-mean-square (rms) errors for the selected subperiods and the entire IOP are about 15% and 20%, respectively, the biases are about 3% and 10%, the correlation coefficients are about 0.6 and 0.4, and the normalized standard deviations are about 1.2. These results suggest that the relative humidity is predicted relatively well by the model. By comparison, Emanuel and Zivkovic-Rothman (1999) optimized a cumulus parameterization's parameters in an SCM by minimizing the rms error of relative humidity. After optimization, the rms error was about 15%.

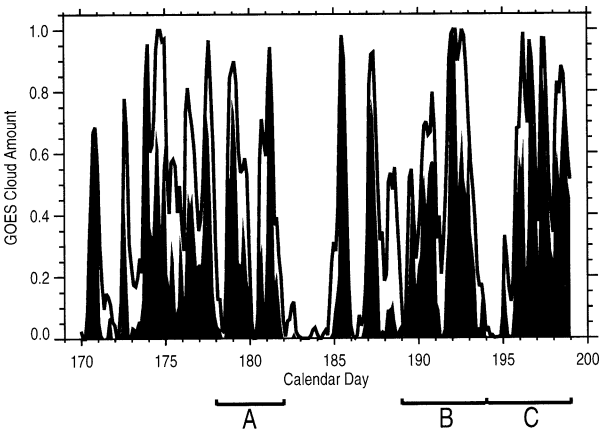

FIG. 1. Time series of GOES observed cloud amounts over ARM SGP CART site for summer 1997 IOP where A, B, and C denote three subperiods of the IOP. The solid line represents the total cloud amount. The shaded area represents the high-cloud amount.

3. Method to use cirrus retrievals to evaluate CRM results

a. Cirrus retrievals

MCA determined the properties of cirrus clouds derived from 1 yr (December 1996–November 1997) of 35-GHz radar (MMCR) data collected at the SGP ARM site in Oklahoma. They also used additional measurements to retrieve the bulk microphysical properties of thin cirrus.

According to MCA, to qualify as a cirrus cloud layer, the temperature at cloud top must be less than -35°C and the temperature at the level of maximum ice water content must be less than -20°C. This definition ensures that ice microphysical processes are dominant in the generation region near cloud top, but excludes deep cloud layers that are capped by ice-phase clouds. MCA used a version of this definition based on radar reflectivity. They required the radar echo top to occur at a temperature less than -35°C and the level of maximum dBZ_e to occur at a temperature less than -20°C. At cirrus cloud levels, the minimum detectable reflectivity of the SGP cloud radar is -40 to -35 dBZ_e. The tem-

[1] The video tape of the animation of GOES IR imagery is available from ARM.

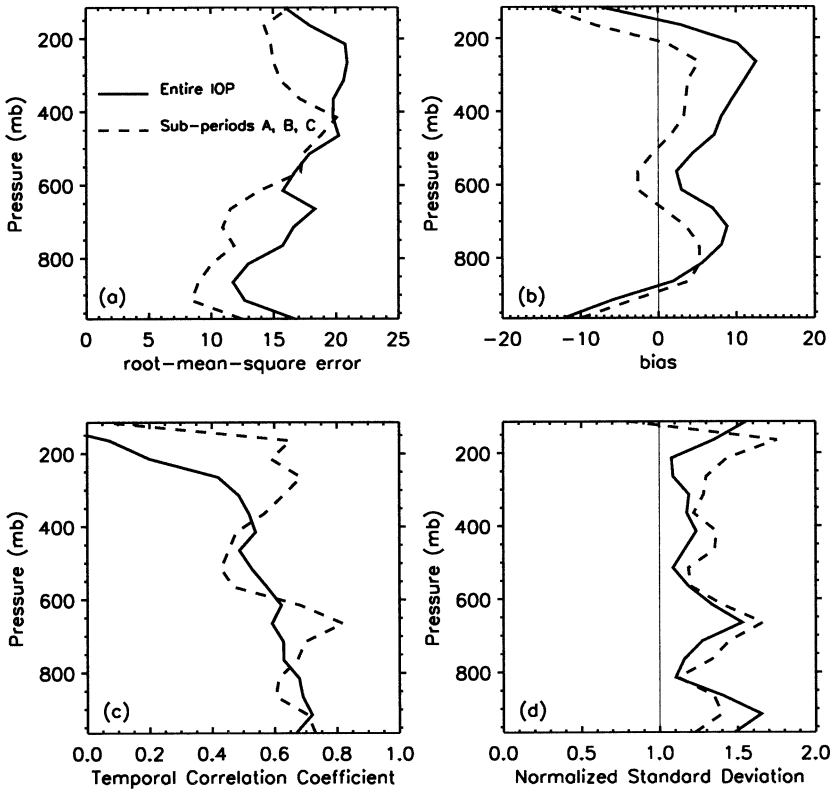

FIG. 2. Statistics of relative humidity for the entire simulation period (solid lines) and the selected subperiods A, B, and C (dashed lines). (a) Rms error. (b) Bias. (c) Temporal correlation coefficient. (d) Normalized std dev.

poral and vertical resolution of the cloud radar is 30 s and 90 m, respectively.

MCA retrieved the ice water path, layer-mean effective radius (r_e), and the layer-mean ice particle concentration (n) using the method described by Mace et al. (1998). The method assumes that the cirrus ice particle size distribution can be described by a first-order modified gamma distribution. The particular size distribution is determined by requiring that its sixth moment match the observed radar reflectivity factor, and that its radiative properties, as parameterized by Fu and Liou (1993), match the radiance measured by the atmospheric emitted radiance interferometer (AERI) at a wavelength between 10.2 to 12.5 μm. This retrieval algorithm requires that the cirrus layer be optically thin, with a layer emissivity less than 0.85. It is also necessary that no lower clouds obscure the cirrus layer from the AERI. The temporal resolution of the retrieved properties is determined by the AERI: 3-min averages are generated every 8 min, so these numbers represent the individual retrievals that are 3-min-averaged layer means. Observational and theoretical studies cited by MCA indicate that the IWP and effective size can be determined within uncertainties of 30% and 20%, respectively.

For a retrieval to be considered reliable, we required that 1) the fractional difference of the retrieved radiance compared to that measured by the AERI be less than 0.1, 2) the IWP be less than 1000 g m^{-2}, and 3) the layer-mean IWC be less than 100 mg m^{-3}. For the summer 1997 (June, July, August) there were 1276 reliable retrievals, which is about 76% of the total retrievals.

b. Simulated cirrus

We sampled the CRM results at 16 grid columns (32 km apart) every 5 min for all 29 days of the simulation using nearly the same definitions of cirrus and ''thin cirrus'' as MCA. To qualify as a cirrus cloud layer in the simulation, we required the radar echo top to occur at a temperature less than -35°C. To be consistent with the SGP cloud radar's sensitivity, we defined a radar echo to exist when $\mathrm{dB}Z_e \geq -40$. The CRM performs microphysical calculations for a hydrometeor species only if its mixing ratio is greater than 10^{-6} kg kg^{-1}. This restricts the snow reflectivity to values greater than about -30 dBZ_e at cirrus cloud levels. We also required the maximum dBZ_e in a cirrus cloud layer to occur at a temperature less than -20°C. To qualify as thin cirrus, we also require the cirrus layer to have an IR emissivity less than 0.85, and for there to be no lower clouds.

We calculated the reflectivity from the mixing ratios of rain, graupel, cloud water, cloud ice, and snow. For

rain and graupel, the reflectivity depends on the intercept and density of each species, as well as the mixing ratio. For cloud water, cloud ice, and snow, the reflectivity depends on the effective radius of the cloud particles and the mixing ratio. The reflectivity for these species is estimated using the following equation suggested by S. Matrosov (Beesley et al. 2000):

$$Z_e = aWr_e^3, \tag{5}$$

where a is a coefficient (49.6×10^{-6} for liquid, 9.4×10^{-6} for ice), W is liquid or ice water content in g m^{-3}, and r_e is an assumed effective radius of the cloud particles in micrometers (Beesley et al. 2000). For ice particles, r_e is the equivalent spherical effective radius defined as the ratio of the third and second moments of the size distribution. The units of the coefficient a are such that W is g m^{-3}, r_e is in micrometers, and Z_e is in mm^6 m^{-3}. The coefficient a depends on the details of the particle size distribution. The suggested values are for the lognormal distribution with width parameter $\sigma = 0.44$ (liquid clouds) and the first-order gamma function distribution (ice clouds) (Matrosov 1999). The coefficient recommended by Matrosov for ice is valid up to about $r_e < 40$–45 μm. For larger r_e it decreases with r_e (this is the effect of the particle bulk density, which diminishes with size). We used $r_e = 10$ μm for cloud water, 25 μm for cloud ice, and 75 μm for snow (Q. Fu 2000, personal communication) to estimate radar reflectivity and IR emissivity. The r_e parameterization was not used in the CRM simulation. It was used only in the analysis to diagnose radiative properties of cirrus.

We calculated the IR emissivity of a cirrus layer from the mixing ratios and effective sizes of cloud ice and snow. The cloud layer IR emissivity ε at a particular wavelength is defined as

$$\varepsilon = 1 - \exp\left[-\int_{z_1}^{z_2} \sigma_a(z)\, dz\right], \tag{6}$$

where

$$\sigma_a(z) = [1 - \tilde{\omega}(z)]\beta(z), \tag{7}$$

is the infrared absorption coefficient, z_1 is the cloud-base height, z_2 is the cloud-top height, $\tilde{\omega}$ is the single-scattering albedo, and β is the extinction coefficient. As parameterized by Fu and Liou (1993), β and $\tilde{\omega}$ can be obtained in terms of the mean effective size and ice water content:

$$\beta = \text{IWC} \sum_{n=0}^{2} a_n/D_e^n \tag{8}$$

$$1 - \tilde{\omega} = \sum_{n=0}^{3} b_n D_e^n, \tag{9}$$

where a_n and b_n are wavelength-dependent coefficients, and D_e is the mean effective size of ice crystals. Fu and Liou gave the coefficients for 18 spectral bands with central wavelengths ranging from 0.55 to 70.0 μm. In order to match the radiance used by MCA (wavelength between 10.2 and 12.5 μm), those coefficients for the spectral band with 11.3-μm central wave length are used in our calculation. To include the emittance of large ice particles (snow) in addition to small ice particles (ice) in cirrus clouds, we used the following equation to calculate σ_a:

$$\sigma_a = [1 - \tilde{\omega}(z)]_i\beta_i(z) + [1 - \tilde{\omega}(z)]_s\beta_s(z). \tag{10}$$

The layer mean D_e is obtained from

$$\overline{D}_e = \frac{\text{IWP} + \text{SWP}}{\dfrac{\text{IWP}}{D_{ei}} + \dfrac{\text{SWP}}{D_{es}}}, \tag{11}$$

where IWP and SWP are ice water path and snow water path, and D_{ei} and D_{es} are effective sizes of cloud ice and snow, respectively. From the formula, we can see that the cirrus layer mean effective size is determined by the specified values of D_{ei} and D_{es}, and the partitioning of ice mass between small (cloud ice) and large (snow) particles in the cirrus clouds. We set $D_e = 2r_e$ by assuming a quasi-spherical shape of ice crystal so that D_e is 50 and 150 μm for ice and snow, respectively. The layer-mean effective radius is then simply

$$\overline{r}_e = \overline{D}_e/2. \tag{12}$$

For the CRM-simulated cirrus cloud layers, we calculated frequency distributions of IWP, IWC, effective radius (r_e), layer thickness, midcloud height, and midcloud temperature using the same criteria as MCA for ''all cirrus'' clouds, thin cirrus clouds, cold thin cirrus, and warm thin cirrus. The cloud type definitions are analogous to those used by MCA. Note that the observational statistics used in our comparison are based on 3 months of cloud property retrievals, from June to August 1997, while the period of our simulation is 29 days starting 2330 UTC 18 June 1997. When cirrus occurrence frequency is examined however, only observations during the SCM IOP, that is, the same period as the CRM simulation, are used.

4. Comparison of cirrus properties between CRM and observation

a. Cirrus cloud occurrence frequency

We calculated the CRM all cirrus and thin cirrus 3-hourly COF for each of the 16 single columns (32 km apart). Here the COF is the fraction of time when cirrus are ''observed'' in the CRM column. The COFs averaged over all 16 columns are calculated as well. The all cirrus and thin cirrus COFs from MCA's results are obtained similarly, but for one column only.

We compared the CRM COF and MCA's COF with the GOES high cloud amount (Minnis et al. 1995). The GOES high cloud amount is area averaged over the SCM domain. The GOES cloud height is based on the

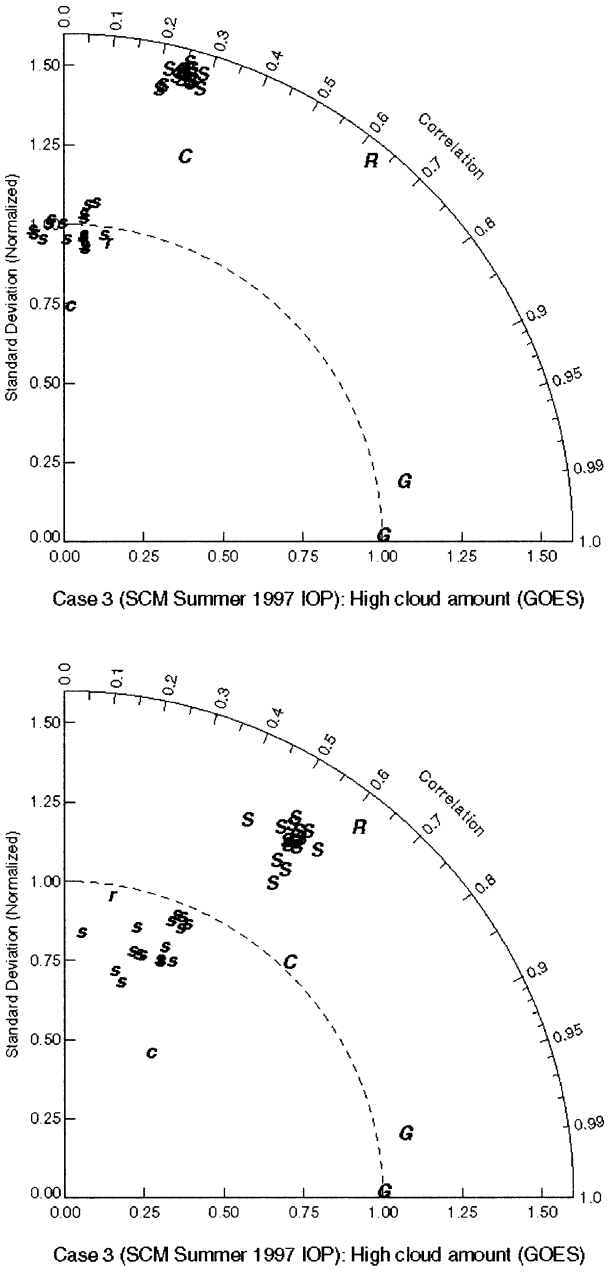

FIG. 3. (a) Taylor diagram for 3-hourly cirrus COF over the entire simulation period. (b) Similar to (a) but for subperiods A, B, and C of the IOP. The reference field is the smoothed GOES high-cloud amount. ***G***: the reference field and the unsmoothed GOES high-cloud amount; ***R*** and ***r***: MCA's all and thin cirrus COF. ***C*** and ***c***: CRM all cirrus and thin cirrus COF averaged over 16 columns. ***S*** and ***s***: CRM all cirrus and thin cirrus COF at 16 single columns.

cloud-center temperature, which is defined as the equivalent radiating temperature of the cloud, assuming the cloud radiates as a blackbody. For optically thin clouds, the cloud-center temperature generally corresponds to some temperature between the physical center and top of the cloud. The cloud-center temperature approaches the cloud-top temperature as the cloud becomes optically thick. A sounding is used to get the cloud-center altitude. High clouds are those with cloud-center altitudes higher than 6 km.

TABLE 1. Cirrus occurrence frequency (values without brakets or parentheses) from the CRM simulation, Mace et al. (2001), and GOES observation at ARM SGP CART site; correlation coefficients (values in brackets) and normalized standard deviation (values in parentheses) with respect to GOES high-cloud amount (version 1).

Period	CRM	MMCR	GOES
Summer 1997 SCM IOP	0.37 [0.30] (1.250)	0.30 [0.63] (1.523)	0.27 [1.00] (1.00)
Subperiods A, B, C	0.30 [0.70] (1.011)	0.37 [0.63] (1.476)	0.34 [1.00] (1.00)

A Taylor diagram can concisely summarize the degree of correspondence between simulated and observed fields or time series (Taylor 2001). It is used here to describe the performance of the CRM in simulating the occurrence of cirrus clouds (Fig. 3). Only observations during the SCM IOP are used here in the comparison. The 3-hourly GOES high-cloud amount observed at the ARM SGP CART site (averaged over 9 h) is used as the reference field. It is represented by a symbol ***G*** located at the point where the correlation is 1.0 and the normalized standard deviation is 1.0 in Fig. 3. The other symbol ***G*** in Fig. 3 represents the unsmoothed GOES high-cloud amount. Since the large-scale forcing used to drive the CRM was obtained by averaging the constraining surface and top-of-atmosphere (TOA) fluxes over 9 h, we compare the CRM results with the smoothed GOES high-cloud amount. To be consistent, we should compare MCA's results with the unsmoothed GOES high-cloud amount. As shown by Fig. 3, however, there is little difference between the statistics of the two GOES high-cloud amounts: their correlation coefficient is 0.99 and the ratio of their standard deviations is 1.08, so it is reasonable to use the smoothed high-cloud amount as the reference field for MCA's results, too.

Table 1 gives the cirrus COFs as well as the corresponding correlation coefficients and standard deviations with respect to the GOES high-cloud amount (averaged over 9 h). Over the entire simulation period, the CRM cirrus COF is 0.37, the radar-observed cirrus COF is 0.30, and the GOES high cloud amount is 0.27. The cirrus occurrence during the subperiods A, B, and C from the CRM-simulated and radar observations are 0.30 and 0.37, respectively, while the high cloud amount from GOES is 0.34. For both the entire IOP and the subperiods, the GOES high-cloud amount is 0.03 less than the cloud radar cirrus COF. The fact that GOES can fail to detect or properly classify optically thin high clouds may partly explain the difference between GOES high cloud and radar cirrus amounts. The CRM cirrus COF during the three subperiods is 0.30, which is slightly less than the cloud radar cirrus COF and the GOES high-cloud amount. The cloud radar cirrus COF and the

GOES high-cloud amount were 0.07 greater during the subperiods than during the entire IOP, while the CRM cirrus COF was 0.07 less during the subperiods than during the entire IOP. The anomalously large CRM cirrus COF for the IOP appears to be primarily due to large-scale forcing errors, as described below.

Barnett et al. (1998) found that a 3-h time average of solar radiation (with diurnal cycle removed) on cloudy days at a single point has a correlation of 0.6 with the average over a region 180 km in diameter. We found the same correlation (0.63) between the cirrus COF observed by the cloud radar and the GOES high-cloud amount averaged over the 300-km diameter SCM domain (both averaged over 3 h), as shown in Table 1 and Fig. 3.

The correlation with GOES high-cloud amount for the CRM all cirrus and thin cirrus COF for the entire IOP averaged over 16 columns, symbols ***C*** and ***c*** in Fig. 3a, are 0.30 and 0.03, respectively, which are lower than the corresponding values for the radar observations and retrievals, 0.63 and 0.15 (symbols ***R*** and ***r***). The CRM cirrus COFs, when averaged over 8 columns (64 km apart) are almost the same as those averaged over 16 columns, so the CRM cirrus cloud occurrence frequency averaged over 8 or more columns can represent the large-scale, or CART-averaged value. For the entire IOP, the CRM all cirrus and thin cirrus COFs at 16 single columns (symbols ***S*** and ***s***) are correlated less with the GOES high clouds amount than are MCA's results. There are some possible reasons for the poor correlation between CRM cirrus occurrence and GOES observation. The lack of estimates of large-scale condensate advection is probably the main reason. Sampling from a single CRM simulation is another reason due to the variability in the convective systems in different simulations. Model deficiencies in the presentation of physical processes, particularly ice microphysics, are of course also a possible reason. Errors in the large-scale forcing used to drive the CRM contribute to the poor correlation between CRM and GOES observation, when the whole period is considered. We compared the time series of CRM simulated cirrus COF, cloud radar observed cirrus COF, and GOES high-cloud amount during the entire simulation period to identify periods of disagreement. We also compared the time series of the upper-tropospheric large-scale vertical velocity used to determine the large-scale advective tendencies used in the CRM simulation (which was obtained by averaging the constraining surface and TOA fluxes over 9 h in the variational analysis), with the unsmoothed time series to determine periods of disagreement that may indicate errors due to averaging. The CRM overestimates cirrus occurrence on 2 and 3 July when strong upward motion occurs in the smoothed analysis (compared with the unsmoothed version), and the overestimation on 5 July is possibly related to the unrealistic weak downward motion.

To largely exclude the effects of no condensate advection estimates, we calculated the statistics for subperiods A, B, and C of the simulation (14 days), during which cloud systems formed and decayed mostly within the CART. The results are shown in Fig. 3b and Table 1. The correlation coefficients for CRM all cirrus and thin cirrus cloud occurrence with respect to GOES high-cloud amount increase to 0.70 and 0.52, respectively, while those for the radar observations and retrievals remain unchanged: 0.63 and 0.15. Apparently the CRM can simulate the occurrence of locally formed cirrus reasonably well in these subperiods. Our analysis of the National Centers for Environmental Prediction SCM cirrus properties also shows that the correlation of the SCM cirrus COF increases significantly when only these subperiods are considered (from 0.47 to 0.68) (Luo et al. 2002). Since the CRM and the SCM contain very different physics, this suggests that lack of cloud water/ice advection is a major reason for the poor temporal correlation between simulated cirrus occurrence and observations over the entire IOP, and that including such advection in numerical models will increase their ability to predict cirrus occurrence.

We should mention that although the temporal correlation between CRM cirrus and the observations over the entire simulation period is low, this should not affect the statistical properties of CRM cirrus clouds since the properties should be determined by the physical processes in the model and the large-scale advective tendencies used to drive the model.

TABLE 2. Cirrus macroscale statistics derived from the CRM simulation over summer 1997 SCM IOP and from Mace et al. (2001) summer 1997 (Jun, Jul, Aug) data at the SGP ARM site. The values outside of brackets or parentheses are mean quantities. Values in parentheses denote std devs of the mean quantities. Values in brackets denote means derived from the optically thin single-layer subset of cloud events. The CRM results are based on samples at eight columns (64 km apart).

	CRM	MCA
Freq. (%)	37	30*
	[19]	[16*]
Base height (km)	8.8 (2.0)	10.3 (1.8)
	[8.9]	[10.8]
Top height (km)	12.0 (1.3)	12.1 (1.4)
	[11.7]	[12.4]
Midcloud height (km)	10.5 (1.3)	11.2 (1.5)
	[10.3]	[11.6]
Thickness (km)	3.4 (2.0)	2.0 (1.5)
	[2.8]	[1.5]
Midcloud temperature (K)	228 (9.4)	225 (10.5)
	[228]	[223]

* The cirrus cloud frequency is obtained using data during the SCM summer IOP.

b. Cirrus macroscale statistics

The macroscale statistics of the simulated and observed cirrus clouds are shown in Table 2. Figures 4 and 5 give frequency distributions of the cirrus macro-

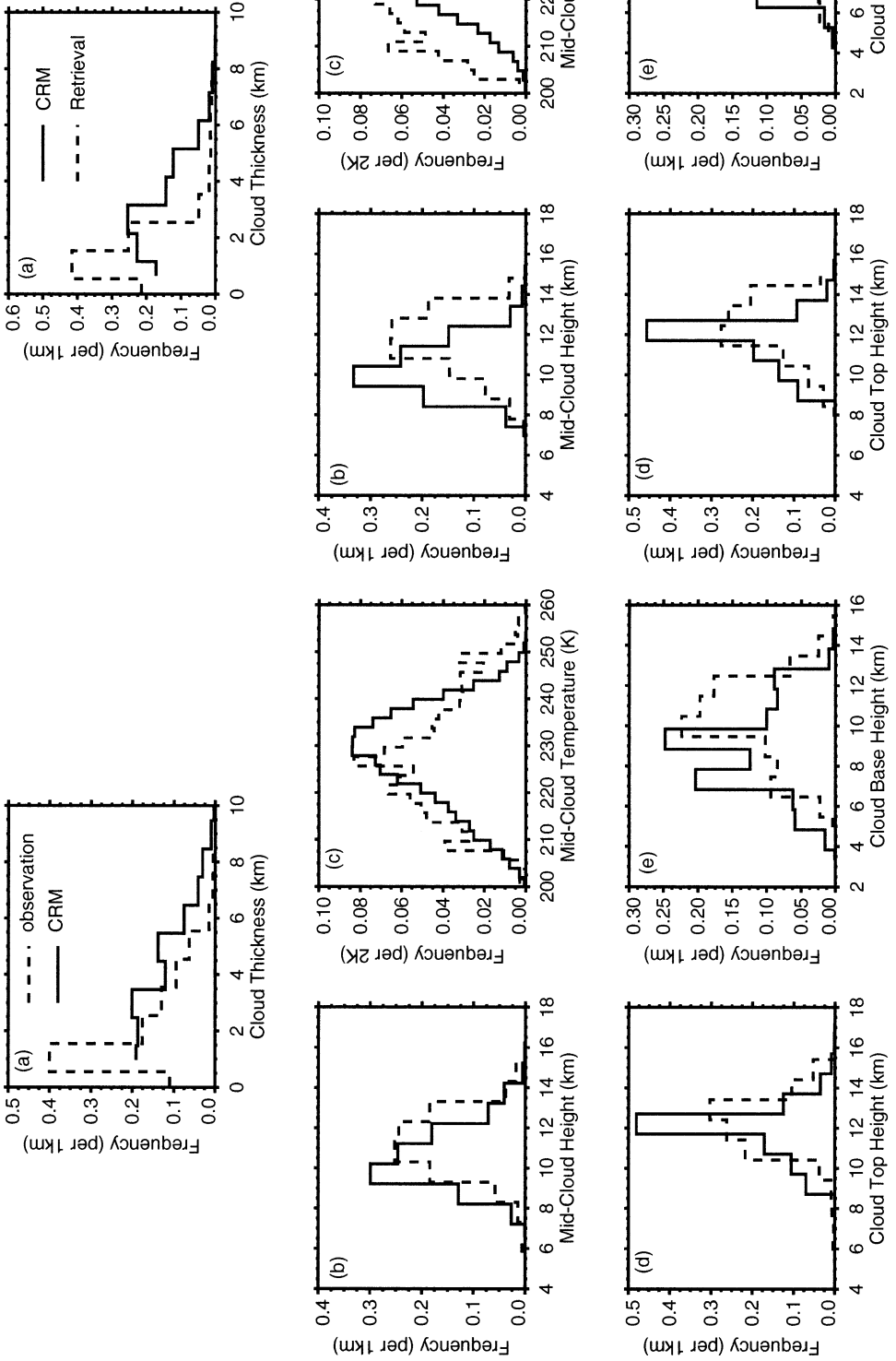

FIG. 4. Frequency distributions of all cirrus macrophysical quantities. Solid line: CRM simulation; dashed line: Mace et al. (2001) summer 1997 dataset. (a) Cloud thickness. (b) Midcloud height. (c) Layer-mean temperature. (d) Cloud-top height. (e) Cloud-base height.

FIG. 5. Similar to Fig. 4 but for thin cirrus clouds.

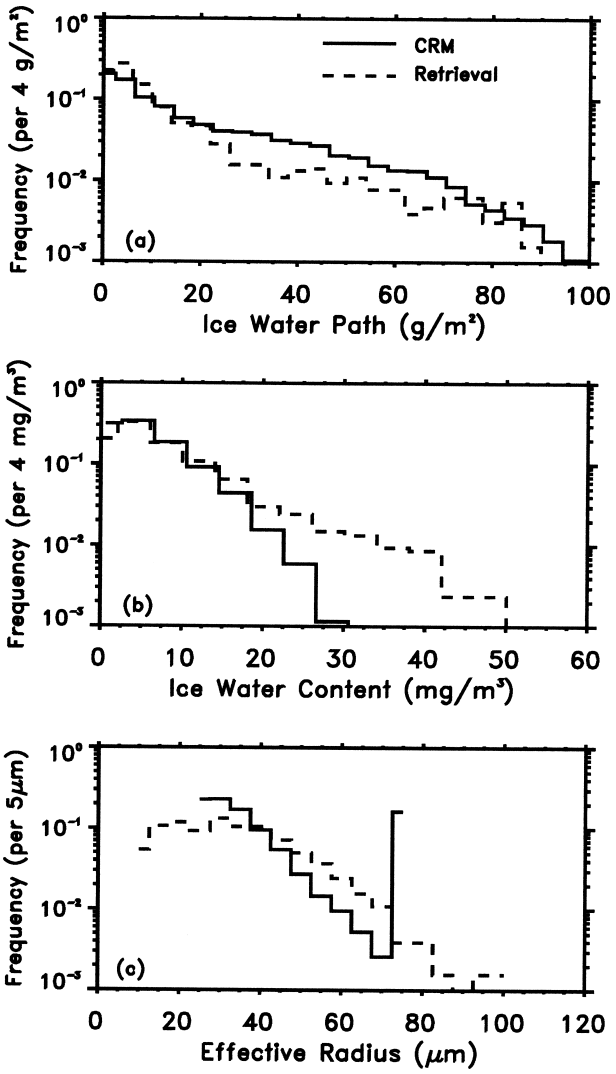

FIG. 6. Frequency distributions of thin cirrus microphysical properties from CRM (solid line) and MCA (dashed line). (a) Ice water path. (b) Layer-mean ice water content. (c) Layer-mean effective radius.

scale statistics for all cirrus and thin cirrus clouds, respectively. The CRM results are based on samples at eight columns (64 km apart) every 5 min for the entire simulation period. For all cirrus we found 24 581 samples in total. For thin cirrus we found 13 062 samples. The MCA dataset of summer 1997 (June, July, and August) are used.

We found that CRM-simulated cirrus tend to have lower base and are thicker. The mean cloud-top and cloud-base heights of CRM all cirrus clouds are 12.0 and 8.8 km, that is, 0.1 and 1.5 km lower, respectively, than the radar observations. The mean thickness is 3.4 and 2.8 km for all cirrus and thin cirrus, respectively, which is larger than radar observations (2.0 and 1.5 km). Comparing the frequency distributions of cloud thickness of CRM cirrus and observed cirrus (Figs. 4a and 5a), we can find that the modal values of the CRM cirrus cloud thickness distribution are both larger than the radar observations. Some of this discrepancy can be explained by the large vertical grid interval of the CRM, which is about 800 m at cirrus levels and about 8 times the cloud radar's vertical grid interval. Since the discrepancies in the CRM's mean cloud base are -1.5 and -1.9 km for all and thin cirrus, respectively, while those of the mean cloud top are smaller, -0.1 and -0.7 km, we expect that one possible reason for too large depths is that the large ice crystals in the CRM cirrus fall too far before evaporating. This could be due to the fall speed of the large-crystal component of the size distribution being too great.

TABLE 3. Thin cirrus microphysical and radiative properties. Values without brackets are the CRM results for summer 1997 SCM IOP while those in brackets denote results from Mace et al. (2001) for summer 1997 (Jun, Jul, Aug). The CRM results are based on samples at eight columns (64 km apart).

	Mean	Standard deviation	Mode	Median
IWP (gm^{-2})	19.8	21.4	2.5	11.4
	[13.9]	[29.5]	[4.0]	[6.0]
$\overline{IWC}$ (mgm^{-3})	5.9	4.9	4.6	4.4
	[8.7]	[9.7]	[4.1]	[5.6]
$\bar{r}_e$ (μm)	40.3	17.1	30.0	33.5
	[43.9]	[50.0]	[30.1]	[32.1]
IR emissivity	0.305	0.257	0.054	0.235
	[0.276]	[0.220]	[0.001]	[0.226]
Visible optical depth	0.877	0.923	0.009	0.510
	[0.554]	[0.667]	[0.202]	[0.324]

The radar-observed and CRM-simulated midcloud height distributions have similar shapes but again the simulated cirrus cloud heights are lower (Figs. 4b and 5b). Given the above results, CRM cirrus clouds tend to be warmer than the observations (Figs. 4c and 5c). Therefore, we can say that, compared with the observations, the CRM cirrus clouds occur at lower heights (higher temperatures) with thicknesses that are too large.

c. Thin cirrus microphysical properties

The radiative properties of cirrus clouds depend on the macroscale and microphysical properties. Frequency distributions of thin cirrus microphysical properties, including ice water path, layer-mean ice water content, and layer-mean effective radius (r_e) are shown in Fig. 6. Table 3 gives the statistics of these properties as well as those of IR emissivity and visible optical depth. We can evaluate these properties for CRM thin cirrus only since the microphysical properties of optically thick cirrus cannot be determined using the retrieval technique of MCA.

Both the observations and the CRM show that most thin cirrus clouds have relatively low IWP and layer-mean IWC. The simulated mean IWP is 19.8 g m^{-2}, which is comparable to the retrieval (13.9 g m^{-2}). The mean layer-mean IWC from the CRM and retrieval are

5.9 and 8.7 mg m^{-3}, respectively. The maxima of both the IWP and IWC distributions show agreement between the simulation and observations. Basically, the distributions of CRM IWP and IWC match those of observations fairly well. The agreement suggests that the CRM produces about the correct amount of ice in its thin cirrus cloud cover. One disagreement here is that some thin cirrus clouds with large IWC (larger than 30 mg m^{-3}) are observed but not simulated by the CRM.

The frequency distribution of layer-mean r_e for the CRM cirrus clouds is unrealistic compared with observation. This occurs because of the simple method we used to specify the effective radius. As noted in section 3b, the effective size in the CRM cirrus clouds is determined by the specified sizes of small ice crystals (25 μm) and large ice crystals (75 μm) as well as the IWP and SWP values in the cirrus cloud. As a result, r_e cannot be smaller than 25 μm, nor larger than 75 μm. A more physically based method for specifying the effective size is needed in order to diagnose the radiative properties of CRM cirrus clouds more realistically. Table 3 also shows that the statistics of layer IR emissivity and visible optical depth of CRM thin cirrus clouds are comparable to those of the observations.

d. Thin cirrus physical relationships

The properties of cirrus clouds that form as a result of large-scale ascent are the result of an approximate balance between ice production by deposition and ice loss due to sedimentation and sublimation (Heymsfield and Donner 1990; Donner et al. 1997). In such circumstances, ice production, P, depends primarily on temperature and large-scale vertical velocity, while sedimentation and sublimation loss, L, depends on the ice mixing ratio, q_i, and the residence time of ice in the layer, τ. The residence time is related to the layer thickness, h, and the ice fall speed, V_i. This process can be represented by the following equation:

$$\frac{dq_i}{dt} = P - L = P - \frac{q_i}{\tau} = P - \frac{q_i V_i}{h} \approx 0. \quad (13)$$

The steady-state ice mixing ratio is $q_i = P(h/V_i)$, and therefore depends on several large-scale parameters (temperature, vertical velocity, and cloud thickness) as well as a microphysical parameter (the ice fall speed). We therefore evaluate the CRM's ability to reproduce the observed relationships between IWC, T, ω, and cloud thickness in thin cirrus.

1) TEMPERATURE AND THICKNESS DEPENDENCE

Due to the impact of adiabatic process on ice cloud content, temperature has been shown to be strongly correlated with observed cirrus properties (e.g., Heymsfield and Platt 1984). It is certainly important to represent such temperature dependency correctly in a CRM. In Fig. 7, we compare the frequency distributions of microphysical properties derived from the observations and simulation, segregated by midcloud temperature (T_m). The right-hand column of plots are for the warm thin cirrus clouds ($T_m > 230$ K), while the left plots are for the cold thin cirrus clouds ($T_m < 220$ K). We found that the observed dependence of the distribution of each property to temperature is qualitatively reproduced by the CRM. The observations show that the mean and median ice water contents tend to increase with midcloud temperature while the modes of the distributions remain near the minimum observation values. Similar results are found in the CRM thin cirrus. Although the distributions of CRM r_e have some unrealistic aspects, the tendency for the CRM mean, median, and mode of r_e to increase with temperature is obvious, and is consistent with the observations.

A plot of thin cirrus IWPs and layer-mean IWCs versus midcloud temperature is given in Fig. 8, which compares CRM results with the results from MCA. The IWPs and layer-mean IWCs are averaged over temperature bins of 5 K. The bar in each temperature bin shows the 90% confidence interval for that temperature range. Figure 8a shows good agreement between the CRM and observed IWP temperature dependence. The rate of increase with temperature and their magnitudes are quite similar. Figure 8b shows that the IWCs generally increase with temperature. The range of the 90% confidence interval for the retrieved results is generally larger than for the CRM results, especially at higher temperature, due to fewer samples. The comparison of the layer-mean IWC–temperature relationships shows that although the CRM and observations have similar rates of increase of IWC, their magnitudes are substantially different with the CRM's being lower. This is consistent because the CRM thin cirrus IWP is about the same as for the retrieved thin cirrus clouds but the CRM thickness is greater (Fig. 5).

Cloud thickness is another important factor determining cirrus properties. Thicker cloud layers most often reach the warmest temperature, so the sensitivity of clouds microphysics on layer-mean temperature implicitly includes a dependence on cloud-layer thickness. However both variables contribute independent information (MCA). The dependence of thin cirrus IWP and layer-mean IWC on cloud thickness in the CRM results is similar to the observed (Table 4). We segregated the thin cirrus layer-mean IWCs and IWPs into three classes (coldest, neutral, and warmest layers) first, and then grouped them by cloud depth ΔZ: $\Delta Z < 1$ km; 1 km $< \Delta Z < 2$ km; 2 km $< \Delta Z < 4$ km. For all three classes (coldest, neutral, and warmest layers), mean and median IWC and IWP values increase significantly when the cloud depth increases from < 1 km to 2–4 km. This feature is found in both the CRM and radar datasets.

Figure 9 is a plot of thin cirrus layer-mean IWCs versus temperature and cloud depth. The IWCs are segregated as in Table 4. The mean value of IWC in each class is represented by a symbol. The bars again indicate

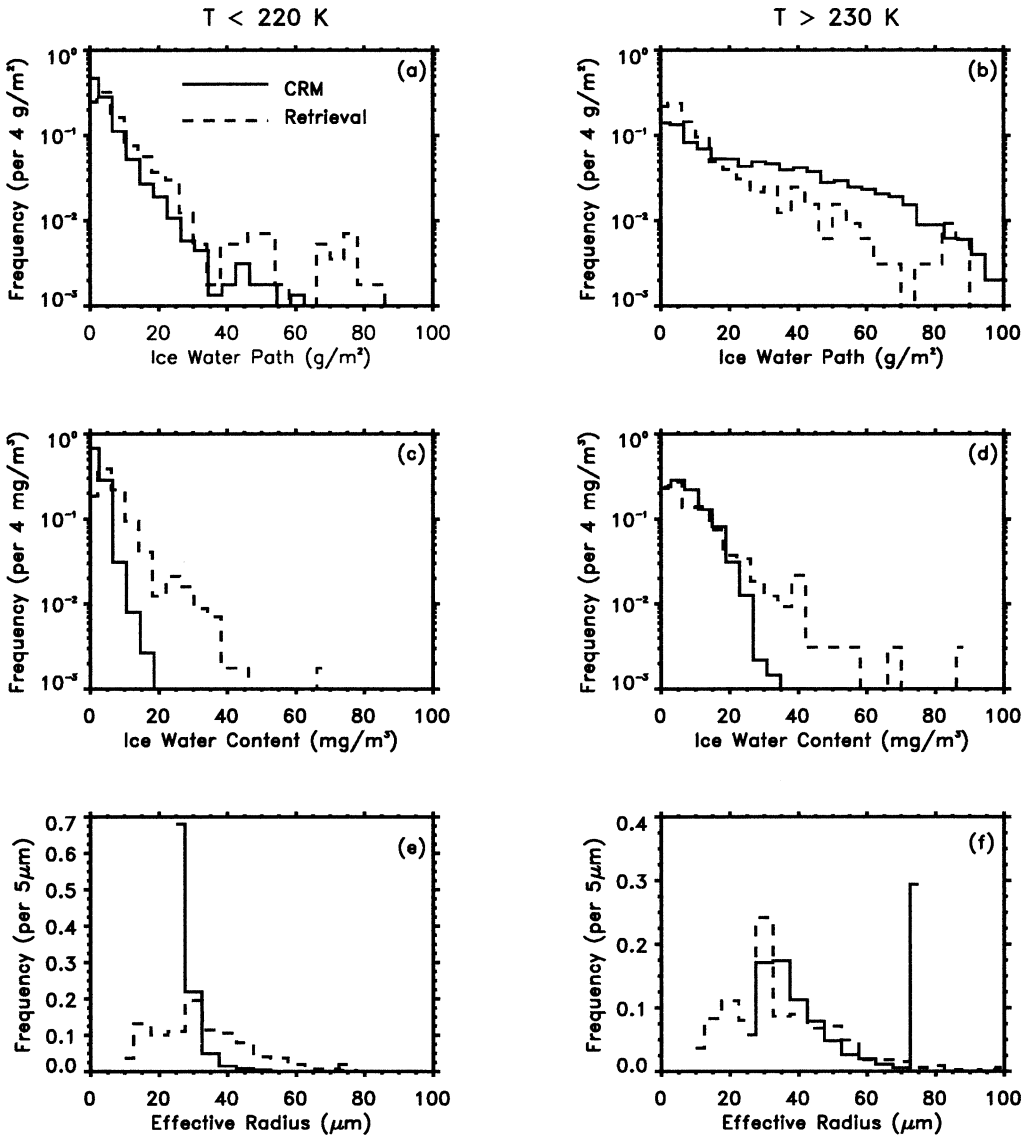

FIG. 7. Frequency distributions of thin cirrus microphysical properties for the warmest and coldest classes. Left plots are for cold layers ($T < 220$ K) and right plots are for warm layers ($T > 230$ K). (top) Ice water path, (middle) layer-mean IWC, (bottom) layer-mean effective radius.

the 90% confidence interval. There is a clear tendency for observed and simulated IWCs to shift toward larger values not only with higher temperature but also for larger cloud thickness, as revealed by both the CRM and retrieval results. The large confidence interval of the retrieval results again from limited samples and also shows the effects of factors other than temperature and cloud depth on IWC.

2) SENSITIVITY TO LARGE-SCALE VERTICAL VELOCITY

We examined the sensitivity of thin cirrus layer-mean IWCs to large-scale vertical velocity for the SCM IOP (Fig. 10). Here the IWCs are 3-hourly averaged values in the thin cirrus cloud classification. The large-scale vertical velocities are 3-hourly $\omega = dp/dt$ at 265-mb level produced by the variational analysis. We used the version of the large-scale ω, which was used to drive the CRM (and was obtained by averaging the constraining flux observations over 9 h) for the CRM IWCs and the unsmoothed version for the retrieved IWCs. The IWCs were first segregated into three classes according to the 265-mb ω: strong subsidence ($\omega > 1$ mb h^{-1}), weak vertical motion (-1 mb h$^{-1} < \omega < 1$ mb h^{-1}), and strong ascent ($\omega < -1$ mb h^{-1}). Then the IWCs were grouped by 3-hourly midcloud temperature into cold layers ($T_m < 220$ K), neutral layers (220 K $< T_m < 230$ K), and warm layers ($T_m > 230$ K). Similar to Fig. 9, the mean value of IWC in each bin is represented

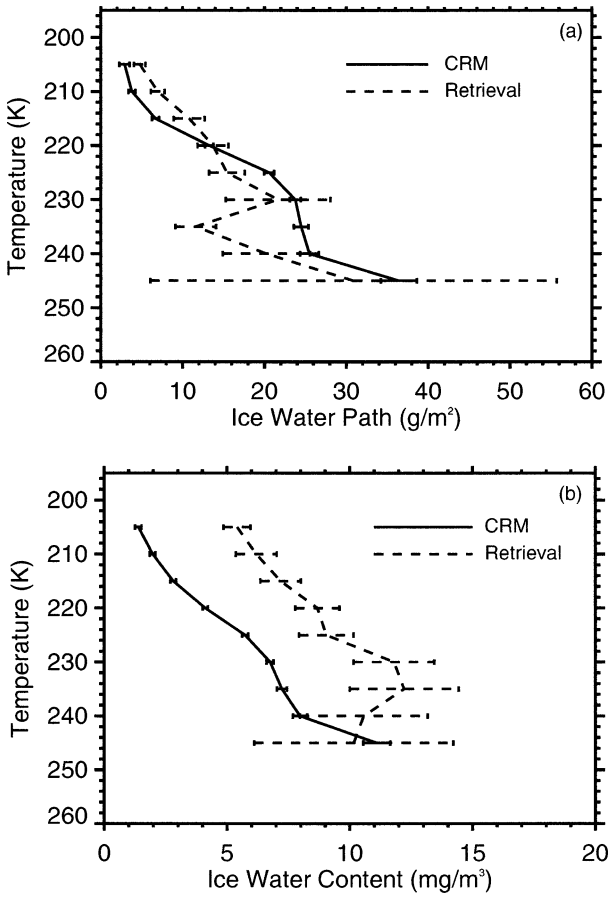

FIG. 8. (a) Thin cirrus IWP vs temperature. (b) Thin cirrus layer-mean IWC vs temperature. The solid line represents CRM results, the dashed line represents MCA's results for summer 1997. The bars are confidence intervals of the mean values within which 90% of the true values lie.

by a symbol (star, triangle, or square) in Fig. 10, and the bar in each bin represents the 90% confidence interval of the mean.

MCA found a weak dependence of thin cirrus IWP on large-scale ascent: the IWP for the largest third of the vertical velocities was significantly greater than that for the smallest two-thirds. Figure 10 shows the observed and CRM dependence of thin cirrus layer-mean IWC on both temperature and large-scale vertical velocity. The weak dependence of IWP on large-scale ascent found by MCA is less evident when the observed thin cirrus properties are further separated into temperature classes, as in Fig. 10. However, the CRM results shown in Fig. 10 both confirm MCA's conclusions and extend them to each of the three temperature classes.

5. Summary and conclusions

CRM-simulated midlatitude cirrus clouds have been little studied due to limited observations. Many cirrus clouds occurred during the ARM summer 1997 IOP over SGP CART. We examined cirrus properties in a CRM simulation driven by the ARM SGP dataset for this period. MCA examined the statistical properties of cirrus clouds based on ground-based cloud radar. We showed that CRM results can be sampled in a way that allows direct comparison to MCA's high-frequency cirrus cloud property retrievals. Because such detailed ground-based cloud radar datasets are now becoming available, this approach allows for evaluation, in a statistical sense, of the CRM's representation of cirrus cloud physical processes.

The CRM results complement and extend the cloud radar observations of cirrus properties. The CRM results are spatially much more extensive than those from the cloud radar. This increases the precision of the physical relationships obtained from the CRM relative to those from the cloud radar because the number of independent atmospheric columns sampled from the CRM simulation is about an order of magnitude greater than sampled by the cloud radar, for a given time period. In addition, the CRM provides coincident results over a large region, so that the spatial variability of cloud properties as a function of horizontal averaging scale can easily be quantified. However, the cloud radar results are absolutely essential because they are needed to evaluate the realism of the CRM results.

When averaged over the entire simulation period, the CRM cirrus COF is slightly larger than the radar observations and GOES high-cloud amount, and temporally poorly correlated with them. However, if we consider only subperiods in which cirrus cloud generation and decay was primarily local, the correlation between CRM and GOES increases significantly and the CRM cirrus occurrence is very close to GOES high-cloud amount. This indicates that the CRM can simulate the local formation and decay of cirrus clouds reasonably well. While errors in the large-scale advective tendencies of potential temperature and water vapor mixing ratio appear to contribute to the inconsistency between CRM cirrus occurrence and the observations, neglecting condensate advection (due to lack of observations) clearly has a detrimental impact on the ability of a model (CRM or large scale) to properly simulate cirrus cloud occurrence. This finding raises concerns for future similar studies since the advective tendency of condensate appears to be very difficult to determine accurately from current available ARM observations. However, satellite retrievals of cirrus properties, including IWP, are increasingly available, and should be used to estimate large-scale ice water advective tendencies. Also, we showed that selecting periods with minimal condensate advection greatly decreases the impact of condensate advection on CRM simulations.

Compared with the cloud radar observations, the CRM cirrus clouds occur at lower heights and with larger thicknesses. One possible reason is that the large ice crystals in the CRM cirrus fall too rapidly. In addition the large CRM vertical grid interval at cirrus levels

TABLE 4. Statistics of the bulk microphysical properties derived from the optically thin single-layer cirrus clouds and segregated by layer depth for the warmest and coldest classes. The value in the upper left is the mean, in the upper right is the std dev, in the lower left is the mode, and in the lower right is the median. Values without brackets are from the CRM simulation for summer 1997 SCM IOP, and values inside the brackets are retrievals from MMCR summer 1997 dataset. The CRM results are based on samples at eight columns (64 km apart).

	Δh	$\overline{\text{IWC}}$ (mg m^{-3})		IWP (g m^{-2})		$\overline{r}_e$ (μm)	
$\overline{T} < 220$ K	<1 km	1.5	0.92	1.2	0.8	27	9
		[5.3]	[5.4]	[3.0]	[2.7]	[19]	[8]
		2.6	1.2	1.5	1.0	25	25
		[4.3]	[4.4]	[4.0]	[2.6]	[15]	[18]
	1–2 km	2.4	1.4	3.8	2.2	28	7
		[7.8]	[6.7]	[11.9]	[11.2]	[30]	[11]
		2.6	2.0	3.1	3.2	25	25
		[4.3]	[6.1]	[4.3]	[8.9]	[27]	[28]
	2–4 km	3.8	2.8	11.0	8.8	30	5
		[9.9]	[9.6]	[23.2]	[22.1]	[37]	[9]
		2.8	3.2	5.9	8.5	30	29
		[4.3]	[6.1]	[8.7]	[15.7]	[38]	[37]
$\overline{T} > 230$ K	<1 km	2.9	3.5	2.1	2.5	55	24
		[12.6]	[9.9]	[5.4]	[7.4]	[37]	[16]
		2.8	1.5	1.6	1.0	75	75
		[4.2]	[5.8]	[2.0]	[2.6]	[30]	[35]
	1–2 km	4.1	4.7	6.1	7.1	60	21
		[13.4]	[10.5]	[17.8]	[16.0]	[49]	[18]
		1.9	2.4	3.3	3.4	75	75
		[2.3]	[11.8]	[4.2]	[15.5]	[34]	[47]
	2–4 km	8.8	5.9	26.1	19.2	47	18
		[11.1]	[8.4]	[31.6]	[26.8]	[62]	[22]
		4.0	7.3	6.1	21.1	75	39
		[5.6]	[9.6]	[9.7]	[28.7]	[42]	[58]

(about 800 m) partly contributes to the larger thickness. Many observed cirrus cloud layers are thinner than 800 m. A smaller vertical grid interval space should be used to simulate thin cirrus clouds. It would be interesting to test the sensitivities of CRM cirrus properties on its vertical resolution and ice fall speed. However, results from such sensitivity experiments are not included since the main goal of this study is to describe and use a new method for using cloud radar data to evaluate a CRM.

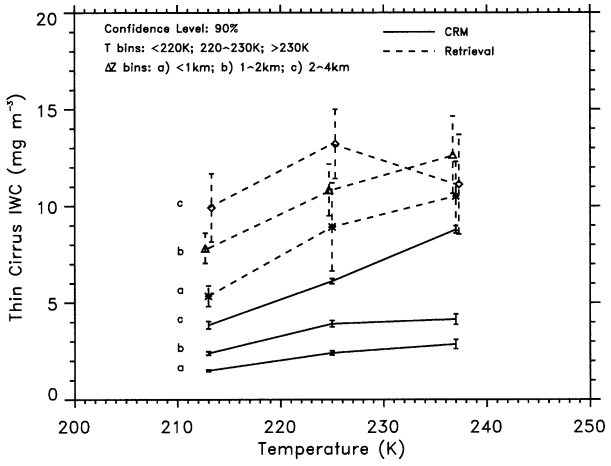

FIG. 9. Thin cirrus layer-mean IWC in terms of temperature and thickness. Solid line: CRM results; dashed line: retrievals for summer 1997. The bars are confidence intervals of the mean values within which 90% of the true values lie.

Some obvious additional potential extensions of this work include 1) determining how all cirrus microphysical properties compare to the thin cirrus properties: are the frequency distributions and physical relationships similar and 2) determining to what extent the properties of convectively generated cirrus differ from cirrus formed in situ.

The frequency distributions of thin cirrus microphysical properties and statistics suggest that the CRM produces about the correct amount of vertically integrated ice in its thin cirrus cloud layers. However, the simulated thin cirrus layers are thicker than observed. As a result, the simulated layer-mean IWC is generally smaller than observed. Although it would have been interesting to do so, we did not use a more complicated microphysical scheme (e.g., a multibin model) in the CRM because one goal of the study is to evaluate the bulk microphysical scheme's performance. In addition, the idealized intercomparison of CRMs made by GCSS Working Group 2 (cirrus clouds) found significant differences between various models, and the ones with more complicated microphysical schemes show just as much scatter as those that used bulk schemes (Starr et al. 2000). At present, it does not appear that the more complicated microphysical schemes give better results.

MCA's results and previous studies indicate that IWP and IWC in cirrus clouds increase with temperature and layer depth. The CRM represents this aspect of cirrus properties quite well. Both the CRM and the observations show that the thin cirrus ice water path during

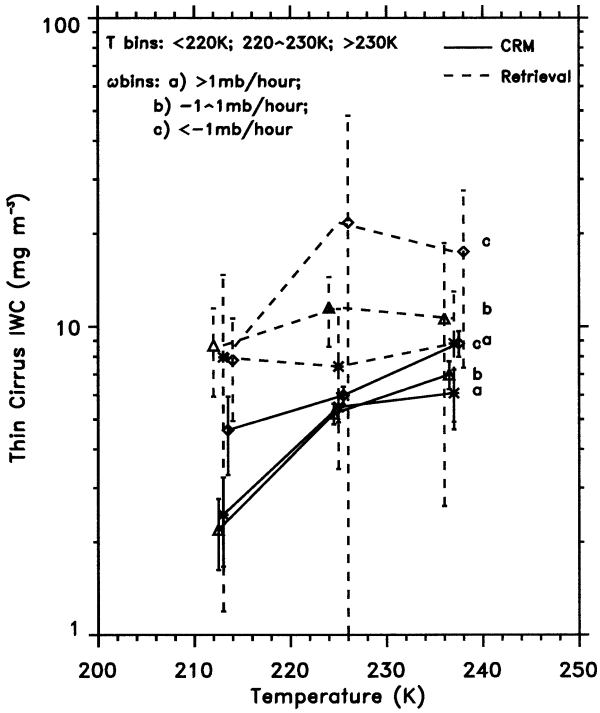

FIG. 10. Thin cirrus layer-mean IWC in terms of temperature and upper-tropospheric large-scale vertical velocity (from the ARM variational analysis). Solid line: CRM results; dashed line: retrievals. The bars are confidence intervals of the mean values within which 90% of the true values lie.

large-scale ascent is only slightly greater than during no ascent or descent.

In anvil cirrus clouds, there may be no ice production due to large-scale vertical motion. Köhler (1999) performed numerical experiments using the UCLA–University of Utah cloud-resolving model to study anvil cloud maintenance and decay under these conditions. Radiation and turbulence were found to have major effects on the lifetime of such cirrus clouds. The optically thick ice clouds decayed significantly slower than would be expected from microphysical crystal fallout alone due to the upward turbulent flux of water that resulted from IR destabilization. Aircraft measurements also indicate that neglecting the cloud-scale circulations in cirrus clouds may underestimate the grid-averaged IWC by a factor of 2 (Donner et al. 1997). The results of these studies, along with MCA's and ours, indicate that further research is warranted to determine the relative importance to cirrus clouds of various scales of vertical motion.

Acknowledgments. This research was supported by the Environmental Sciences Division of the U.S. Department of Energy (DOE) as part of the Atmospheric Radiation Measurement program, under Grants DE-FG03-94ER61769) (Luo and Krueger), DE-FG03-98ER62571 (Mace), and DE-FG03-95ER61968 (Xu, to Colorado State University). Xu's work was also partly supported by the NASA Earth Observation System Interdisciplinary Science Program. The computations were performed at the National Energy Research Supercomputer Center (NERSC), Berkeley, California, which is supported by the Office of Energy Research of the U.S. DOE. Two anonymous reviewers made helpful suggestions of the original manuscript. The authors thank Sally Benson and Erik Vernon for their assistance in obtaining the cloud radar data.

REFERENCES

Barnett, T. P., J. Ritchie, J. Foat, and G. Stokes, 1998: On the space–time scales of the surface solar radiation field. *J. Climate,* **11,** 88–96.

Beesley, T. A., C. S. Bretherton, C. Jakob, E. L Andreas, J. M. Intrieri, and T. A. Uttal, 2000: A comparison of cloud and boundary layer variables in the ECMWF forecast model with observations at Surface Heat Budget of the Arctic Ocean (SHEBA) ice camp. *J. Geophys. Res.,* **105,** 12 337–12 349.

Bony, S., K. M. Lau, and Y. C. Sud, 1997: Sea surface temperature and large-scale circulation influences on tropical greenhouse effect and cloud radiative forcing. *J. Climate,* **10,** 2055–2077.

Brown, P. R. A., and A. J. Heymsfield, 2001: The microphysical properties of tropical convective anvil cirrus: A comparison of models and observations. *Quart. J. Roy. Meteor. Soc.,* **127,** 1535–1550.

Browning, K. A., 1993: The GEWEX Cloud System Study (GCSS). *Bull. Amer. Meteor. Soc.,* **74,** 387–399.

Businger, J. A., J. C. Wyngaard, Y. Izumi, and E. F. Bradley, 1971: Flux–profile relationships in the atmospheric surface layer. *J. Atmos. Sci.,* **28,** 181–189.

Donner, L. J., C. J. Seman, B. J. Soden, R. S. Hemler, J. C. Warren, J. Strooem, and K. N. Liou, 1997: Large-scale ice clouds in the GFDL SKYHI general circulation model. *J. Geophys. Res.,* **102,** 21 745–21 768.

Emanuel, K., and M. Zivkovic-Rothman, 1999: Development and evaluation of a convection scheme for use in climate models. *J. Atmos. Sci.,* **56,** 1766–1782.

Fu, Q., and K. N. Liou, 1993: Parameterization of the radiative properties of clouds. *J. Atmos. Sci.,* **50,** 2008–2025.

——, S. K. Krueger, and K. N. Liou, 1995: Interactions of radiation and convection in simulated tropical cloud clusters. *J. Atmos. Sci.,* **52,** 1310–1328.

Gunn, K. L. S., and J. S. Marshall, 1958: The distribution with size of aggregate snowflakes. *J. Meteor.,* **15,** 452–461.

Harshvardhan, R. Davies, D. A. Randall, and T. G. Corsetti, 1987: A fast radiation parameterization for general circulation models. *J. Geophys. Res.,* **92,** 1009–1016.

Heymsfield, A. J., and C. M. Platt, 1984: A parameterization of the particle size spectrum of ice clouds in terms of the ambient temperature and the ice water content. *J. Atmos. Sci.,* **41,** 846–855.

——, and L. J. Donner, 1990: A scheme for parameterizing ice-cloud water content in general circulation models. *J. Atmos. Sci.,* **47,** 1865–1877.

Hsie, E. Y., R. D. Farley, and H. D. Orville, 1980: Numerical simulation of ice phase convective cloud seeding. *J. Appl. Meteor.,* **19,** 950–977.

Khairoutdinov, M. F., and D. A. Randall, 2001: A cloud resolving model as a cloud parameterization in the NCAR Community Climate System Model: Preliminary results. *Geophys. Res. Lett.,* **28,** 3617–3620.

Klein, S. A., and C. Jakob, 1999: Validation and sensitivities of frontal clouds simulated by the ECMWF model. *Mon. Wea. Rev.,* **127,** 2514–2531.

Köhler, M., 1999: Explicit prediction of ice clouds in general circulation models. Ph.D. dissertation, University of California, Los

Angeles, 167 pp. [Available from Department of Atmospheric Sciences, University of California, 405 Hilgard Ave., Los Angeles, CA 90095.]

Krueger, S. K., 1988: Numerical simulation of tropical cumulus clouds and their interaction with the subcloud layer. *J. Atmos. Sci.,* **45,** 2221–2250.

——, G. T. McLean, and Q. Fu, 1995a: Numerical simulation of the stratus-to-cumulus transition in the subtropical marine boundary layer. Part I: Boundary-layer structure. *J. Atmos. Sci.,* **52,** 2839–2850.

——, ——, and ——, 1995b: Numerical simulation of the stratus-to-cumulus transition in the subtropical marine boundary layer. Part II: Boundary-layer circulation. *J. Atmos. Sci.,* **52,** 2851–2868.

——, Q. Fu, K. N. Liou, and H.-N. S. Chin, 1995c: Improvements of an ice-phase microphysics parameterization for use in numerical simulations of tropical convection. *J. Appl. Meteor.,* **34,** 281–287.

Lau, N.-C., and M. W. Crane, 1997: Comparing satellite and surface observations of cloud patterns in synoptic-scale circulation systems. *Mon. Wea. Rev.,* **125,** 3172–3189.

Lin, Y. L., R. D. Farley, and H. D. Orville, 1983: Bulk parameterization of the snow field in a cloud model. *J. Climate Appl. Meteor.,* **22,** 1065–1092.

Liou, K. N., 1986: Influence of cirrus clouds on weather and climate processes: A global perspective. *Mon. Wea. Rev.,* **114,** 1167–1199.

Locatelli, J. D., and P. V. Hobbs, 1974: Fall speeds and masses of solid precipitation particles. *J. Geophys. Res.,* **79,** 2185–2197.

Lord, S. J., H. E. Willoughby, and J. M. Piotrowicz, 1984: Role of a parameterized ice-phase microphysics in an axisymmetric tropical cyclone model. *J. Atmos. Sci.,* **41,** 2836–2848.

Luo, Y., S. K. Krueger, S. Moorthi, and H.-L. Pan, 2002: Evaluation of cirrus properties simulated by a single-column model using cloud radar observations and results from a cloud-resolving model simulation. Preprints, *11th Conf. on Cloud Physics,* Ogden, UT, Amer. Meteor. Soc., CD-ROM, P3.17.

Mace, G. G., T. P. Ackerman, P. Minnis, and D. F. Young, 1998: Cirrus layer microphysical properties derived from surface-based millimeter radar and infrared interferometer data. *J. Geophys. Res.,* **103,** 23 207–23 216.

——, E. E. Clothiaux, and T. P. Ackerman, 2001: The composite characteristics of cirrus clouds: Bulk properties revealed by one year of continuous cloud radar data. *J. Climate,* **14,** 2185–2203.

Matrosov, S. Y., 1999: Retrievals of vertical profiles of ice cloud microphysics from radar and IR measurements using tuned regressions between reflectivity and cloud parameters. *J. Geophys. Res.,* **104,** 16 741–16 753.

Minnis, P., W. L. Smith Jr., D. P. Garber, J. K. Ayers, and D. R. Doelling, 1995: Cloud properties derived from *GOES-7* for spring 1994 ARM intensive observation period using version 1.0.0 of ARM satellite data analysis program. NASA Reference Publication 1366, NASA Langley Research Center, Hampton, VA, 58 pp.

Norris, J. R., and C. P. Weaver, 2001: Improved techniques for evaluating GCM cloudiness applied to the NCAR CCM3. *J. Climate,* **14,** 2540–2550.

Petch, J. C., and J. Dudhia, 1998: The importance of the horizontal advection of hydrometers in a single-column model. *J. Climate,* **11,** 2437–2452.

Starr, D. O'C., and S. K. Cox, 1985: Cirrus clouds. Part I: A cirrus cloud model. *J. Atmos. Sci.,* **42,** 2663–2681.

——, and Coauthors, 2000: Comparison of cirrus cloud models: A project of the GEWEX Cloud System Study (GCSS) working group on cirrus cloud systems. *Proc. 13th Int. Conf. on Clouds and Precipitation,* Reno, NV, International Association of Meteorology and Atmospheric Sciences, 1–4.

Stephens, G. L., S.-C. Tsay, P. W. Stackhouse Jr., and P. J. Flatau, 1990: The relevance of the microphysical and radiative properties of cirrus clouds to climate and climate feedback. *J. Atmos. Sci.,* **47,** 1742–1753.

Stokes, G. M., and S. E. Schwartz, 1994: The Atmospheric Radiation Measurement (ARM) Program: Programmatic background and design of the Cloud and Radiation Test bed. *Bull. Amer. Meteor. Soc.,* **75,** 1201–1221.

Taylor, K. E., 2001: Summarizing multiple aspects of model performance in a single diagram. *J. Geophys. Res.,* **106,** 7183–7192.

Tselioudis, G., Y. Zhang, and W. B. Rossow, 2000: Cloud and radiation variations associated with northern midlatitude low and high sea level pressure regimes. *J. Climate,* **13,** 312–327.

Xu, K.-M., and S. K. Krueger, 1991: Evaluation of cloudiness parameterizations using a cumulus ensemble model. *Mon. Wea. Rev.,* **119,** 342–367.

——, and A. Arakawa, 1992: Semiprognostic tests of the Arakawa–Schubert cumulus parameterization using simulated data. *J. Atmos. Sci.,* **49,** 2421–2436.

——, and D. A. Randall, 1995: Impact of interactive radiative transfer on the macroscopic behavior of cumulus ensembles. Part I: Radiation parameterization and sensitivity tests. *J. Atmos. Sci.,* **52,** 785–799.

——, and ——, 1996: A semiempirical cloudiness parameterization for use in climate models. *J. Atmos. Sci.,* **53,** 3084–3102.

——, and ——, 2000: Cloud resolving model simulation of the July 1997 IOP: Comparison with ARM data on short, medium, and long subperiods. *Proc. 10th Atmospheric Radiation Measurement (ARM) Science Team Meeting,* San Antonio, TX, Atmospheric Radiation Measurement Program. [Available online at http://www.arm.gov/docs/documents/technical/conf_0003/xu-km.pdf.]

——, A. Arakawa, and S. K. Krueger, 1992: The macroscopic behavior of cumulus ensemble simulated by a cumulus ensemble model. *J. Atmos. Sci.,* **49,** 2402–2420.

——, and Coauthors, 2002: An intercomparison of cloud-resolving models with the ARM summer 1997 IOP data. *Quart. J. Roy. Meteor. Soc.,* **128,** 593–624.

Zhang, M. H., and J. L. Lin, 1997: Constrained variational analysis of sounding data based on column-integrated budgets of mass, heat, moisture, and momentum: Approach and application to ARM measurements. *J. Atmos. Sci.,* **54,** 1503–1524.

——, ——, R. T. Cederwall, J. J. Yio, and S. C. Xie, 2001: Objective analysis of ARM IOP data: Method and sensitivity. *Mon. Wea. Rev.,* **129,** 295–311.